Journal of Maps

ISSN: (Print) (Online) Journal homepage: www.tandfonline.com/journals/tjom20

Geology, U-Pb dating and 3D visualisation of late-orogenic Klenov Pluton (Pelhřimov Core Complex, Central European Variscides)

Jaroslava Pertoldová, Kryštof Verner, David Buriánek, Jan Valenta, Barbora Dudíková, Zuzana Skácelová, Jan Jelének, Jan Jelínek, Kenneth Johnson, Otmar Petyniak & Petra Hejtmánková

To cite this article: Jaroslava Pertoldová, Kryštof Verner, David Buriánek, Jan Valenta, Barbora Dudíková, Zuzana Skácelová, Jan Jelének, Jan Jelínek, Kenneth Johnson, Otmar Petyniak & Petra Hejtmánková (2024) Geology, U-Pb dating and 3D visualisation of late-orogenic Klenov Pluton (Pelhřimov Core Complex, Central European Variscides), Journal of Maps, 20:1, 2317144, DOI: 10.1080/17445647.2024.2317144

To link to this article: https://doi.org/10.1080/17445647.2024.2317144

JOURNAL OF MAPS
2024, VOL. 20, NO. 1, 2317144
https://doi.org/10.1080/17445647.2024.2317144

Geology, U-Pb dating and 3D visualisation of late-orogenic Klenov Pluton (Pelhřimov Core Complex, Central European Variscides)

Jaroslava Pertoldová[a], Kryštof Verner[a,b], David Buriánek[a], Jan Valenta[c,d], Barbora Dudíková[a], Zuzana Skácelová[a], Jan Jelének[a], Jan Jelínek[a], Kenneth Johnson[e], Otmar Petyniak[a] and Petra Hejtmánková[a]

[a]Czech Geological Survey, Prague, Czech Republic; [b]Institute of Petrology and Structural Geology, Charles University, Prague, Czech Republic; [c]Faculty of Science, Institute of Engineering Geology, Hydrogeology and Applied Geophysics, Charles University, Prague, Czech Republic; [d]Institute of Rock Structure and Mechanics, Czech Academy of Sciences, Prague, Czech Republic; [e]Department of Natural Sciences, University of Houston-Downtown, Houston, TX, USA

ABSTRACT

The geological map of the Klenov Pluton (Moldanubian Batholith), and its 3D visualization, brings the new findings in the context of granite emplacement within late-Variscan settings. The Klenov Pluton has a peraluminous composition resulting from partial melting of metasedimentary sources and subsequent differentiation. The new ages 327.14 ± 0.21 Ma and 327.80 ± 0.37 Ma, reflect the narrow time-span of magma emplacement and cooling. The 327 Ma Klenov Pluton was emplaced syntectonically as a 'sheet-like' granite intrusion at depth ca. 10 kilometers during the later stages of the Pelhřimov Core Complex exhumation (at ca. 329 to 327 Ma) associated with ~N–S oriented compression. Gravity modelling suggests that the Klenov Pluton has an asymmetric shape where its western flank is parallel to the ~NW moderately dipping Pelhřimov Core Complex. The eastern margin of the Pluton is shallower and has been later modified by ~SE-side-up normal faulting (Lodhéřov Fault Zone).

ARTICLE HISTORY
Received 12 September 2023
Revised 3 January 2024
Accepted 5 February 2024

KEYWORDS
Bohemian Massif; Moldanubian Zone; Klenov Pluton; geological map; fabric pattern; geophysical survey

1. Introduction

Comprehensive research of granite plutons enables both an interpretation of petrogenesis, fabric pattern and emplacement mechanisms, often in the context of regional geodynamic evolution and the timing of orogenic or magmatic processes, as well as a 3D visualization of the granite intrusion (e.g. Bouchez et al., 2013; Castro et al., 1999; Eshaghi et al., 2020 and references therein). Such results can then bring many useful implications for subsequent applied research. There are numerous studies focused on the use of geothermal energy and sustainable groundwater resources (e.g. Chandrasekharam & Ranjith Pathegama, 2020; Chen et al., 2015; Feng et al., 2020; Shao et al., 2015), mineral deposits assessment (e.g. Eshaghi et al., 2020) and applied research of granitoids for building underground repositories for radioactive waste (e.g. Mattila & Viola, 2014; Soejono et al., 2021; Tóth, 2018; Wang et al., 2018). In this context, under Article No. 23 of Directive EU2011/70/EURATOM, it is widely accepted that the safe and sustainable way for radioactive waste management is the construction of deep geological repositories in granite rock (Vondrovic et al., 2021).

Based on detailed geological and structural mapping on a 1:10,000 scale, remote sensing analysis, gravity modelling, seismic tomography and electrical resistivity tomography (ERT) the geological map on a 1:30,000 scale and 3D visualization of the Klenov Pluton (Moldanubian Batholith; Bohemian Massif) was compiled (Main Map). Further, in combination with new geochemical and petrological data and U-Pb TIMS monazite dating of the Klenov Pluton, we consider the time-frame and geodynamic scenario of the Variscan, late-orogenic LP–HT event and related magmatic activity within the Moldanubian Zone (Central European Variscides).

2. Geological setting

The Klenov Pluton and its high-grade host rocks, belonging to the migmatite-granite Pelhřimov Core Complex, Central European Variscides (Figure 1(a, b); Main Map), recorded relevant events during the late-Varican orogenic episode in the Moldanubian

CONTACT Kryštof Verner krystof.verner@geology.cz Czech Geological Survey, Klárov 3, Prague, 11821, Czech Republic Institute of Petrology and Structural Geology, Charles University, Albertov 6, Prague, 12843, Czech Republic
Supplemental map for this article can be accessed at https://doi.org/10.1080/17445647.2024.2317144

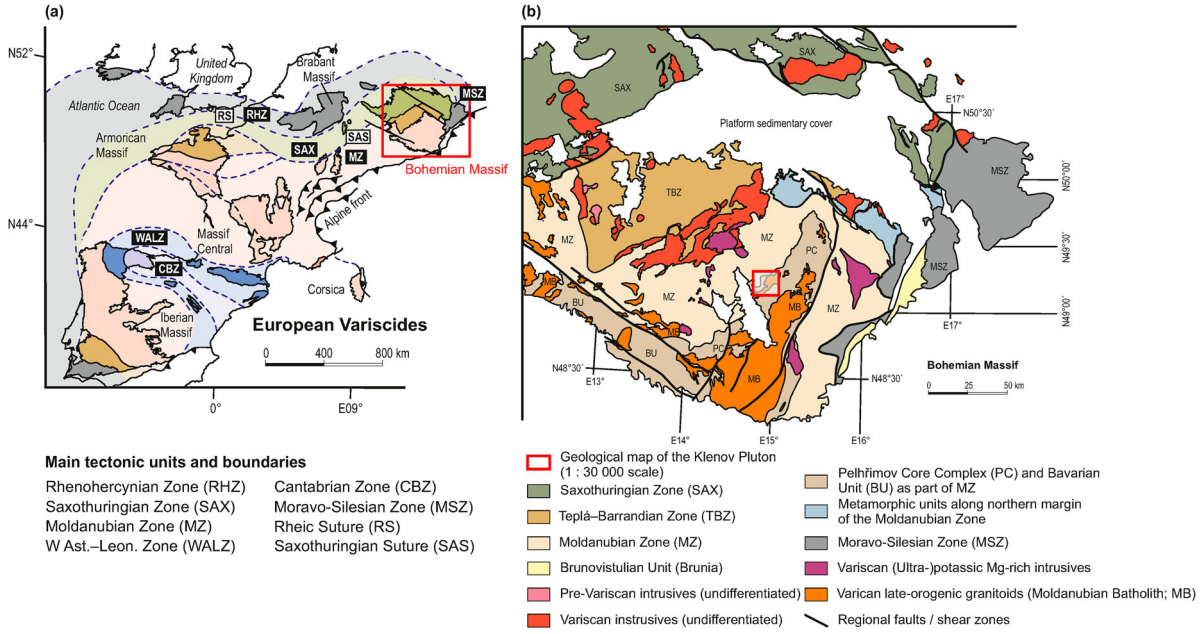

Figure 1. (a) Simplified sketch map of the European Variscides and position of the Bohemian Massif; (b) Simplified geological map of the Bohemian Massif including the geological map of the Klenov Pluton (Main Map).

Zone (see Megerssa et al., 2022; Verner et al., 2014; Žák et al. 2011, 2019 and references therein). The Moldanubian Zone is an exhumed orogenic root domain where several tectonometamorpic events have been recorded (e.g. Megerssa et al., 2022; Schulmann et al., 2009; Žák et al., 2014). The protholith of Moldanubian rocks consists of Neoproterozoic to early Paleozoic igneous and siliciclastic sources affected by MP/LP–HT metamorphism that resulted in abundant sillimanite- and cordierite-bearing migmatites and other rocks with a substantial amount of lower-crustal, high-pressure components such as granulites, eclogites and peridotites (e.g. Fiala et al., 1995; Franke, 1989, 2000; Košler et al., 2014; Matte et al., 1990; Štípská et al., 2004; Tajčmanová et al., 2006). The overall geological architecture of the Moldanubian Zone (Figure 1 (b)) results from the interplay of several geodynamic events (e.g. Brandmayer et al., 1995; Edel et al., 2003; Finger et al., 2007, 2022; Kalvoda et al., 2008; Megerssa et al., 2022; Schulmann et al., 2009; Schulmann & Gayer, 2000; Verner et al., 2014; Winchester et al., 2002; Žák et al. 2011, 2014, 2019): (a) early subduction(s) followed by ~E–W oriented continental collision and prograde MP/(U)HP metamorphism (ca. 380 to 346 Ma), (b) rapid exhumation of deep-seated rocks associated with an extensive HT/MP(LP) isothermal overprint (ca. 345 to 335 Ma), (c) a late-orogenic stage associated with ~N–S shortening, increasing heat flow and extensive anatexis (ca. 335 to 325 Ma) and (d) post-collisional ~ENE–ESW extension, cooling and localized right-lateral shearing along ~NW(WNW)–SE(ESE) and ~NE(NNE)–SW(SSW) striking shear zones (ca. 325 to 300 Ma). Large volumes of peraluminous, two mica granite (known as 'Eisgarn-type granitoids') comprise the prevailing part of the eastern Moldanubian Batholith, and is called the 'Eisgarn Composite Pluton (ECP)'. The ECP includes individual granite bodies such as the Melechov pluton, the 327 Ma Mrákotín Composite Pluton, the Klenov Pluton and the Čiměř pluton (for review see Klomínský et al., 2010 and references therein). These plutons were emplaced into the partly exhumed biotite–sillimanite (± cordierite) migmatites and migmatized paragneisses of the Pelhřimov Core Complex (Verner et al., 2014; Žák et al. 2011, 2019). The Pelhřimov Core Complex (Figure 1(b)) is a roughly ~NNE–SSW oriented granite-migmatite domal structure (Verner et al., 2014; Žák et al. 2011, 2019). This unit underwent extensive anatexis at ca. 329 to 328 Ma at 0.6 GPa and 730°C followed by isothermal decompression and 'gravity-driven' exhumation in the form of a ~NNE–SSW elongated asymmetric domal structure to about 0.2 Gpa within 2–3 M.y., in the context of the waning oblique underthrusting of the Brunia microcontinent (Verner et al., 2014; Žák et al., 2011, 2019).

The Klenov pluton (~22×6 km; Figure 1(b)) crops out along the western margin of the Pelhřimov Core Complex (Verner et al., 2014). The pluton is composed of several facies of peraluminous granite resulting from the partial melting of metasedimentary sources at very high temperatures (René, 1999, 2005; René, 2020). Uranium-rich hydrothermal mineralization occurs along ~NNW–SSE trending faults, designated as the Okrouhlá Radouň Ore Deposit (Dolníček & Krobot, 2013; Fiala & Čadek, 1981; René, 2005).

3. Petrology of granites

The Klenov Pluton is composed of three textural types (facies) of granite (Main Map; Figure 2(a–d)): (a) Equigranular to weakly porphyritic granite (Deštná Granite), (b) porphyritic granite (Dívčí Kopy Granite), and (c) medium to fine-grained granite (Radouň Granite). The prevailing lithology in the Klenov Pluton is equigranular, fine to medium-grained muscovite-biotite, weakly porphyritic granite (Deštná type), which is composed of K-feldspar, quartz, plagioclase, muscovite and biotite (Figure 2(a)). Andalusite occurs as subhedral, pink-coloured grains 0.1–0.2 mm in size or grain aggregates. Rare grains of anhedral cordierite were partly replaced by pinite and/or medium to fine-grained biotite and muscovite. Accessory minerals are represented by apatite, ilmenite, xenotime, monazite, zircon and uraninite (Figure 2(b)). Based on accessory mineral content (monazite, zircon and uraninite), the Deštná type has been divided into two 'subtypes' I and II with different U/Th ratios in whole-rock chemical analysis. The medium-grained, porphyritic muscovite-biotite granite (Dívčí Kopy Granite) occurs as small irregular bodies in the NE flank of the Klenov Pluton. The Dívčí Kopy type is composed of K-feldspar (phenocrysts up to 20 mm in size), plagioclase, quartz, biotite and muscovite (Figure 2(c)). Andalusite was found as muscovite pseudomorphs. Common accessory phases are ilmenite, apatite, zircon, monazite and xenotime. The medium to fine-grained granite (Radouň type) forms veins or irregular intrusions in the Deštná type or surrounding migmatites. This granite consists of anhedral quartz, subhedral plagioclase partly affected by secondary alteration, subhedral to euhedral K-feldspar, biotite and poikilitic cordierite usually replaced by muscovite and chlorite (Figure 2 (d)). The common accessory minerals are sillimanite, apatite, zircon, monazite and xenotime. The monazite-(Ce) and xenotime-(Y) grains are mostly subhedral to euhedral, up to 100 μm in size.

4. Geochemistry

The granites of the Klenov Pluton are characterized by a high content of SiO_2 (69.5–75.2 wt.%), K_2O (3.9–5.3 wt.%) and Na_2O (3.0–4.7 wt.%) with K_2O/Na_2O ratios from 0.8 to 1.7. The Dívčí Kopy type reveals a relatively high content of MgO (0.80–0.93 wt.%) in comparison to the widespread Deštná type (0.09–0.49 wt.%). According to the Q'-ANOR diagram, the granites of the Dívčí Kopy and Deštná II subtype are classified as monzogranite, whereas the Deštná I subtype varies in composition from alkali-feldspar granite

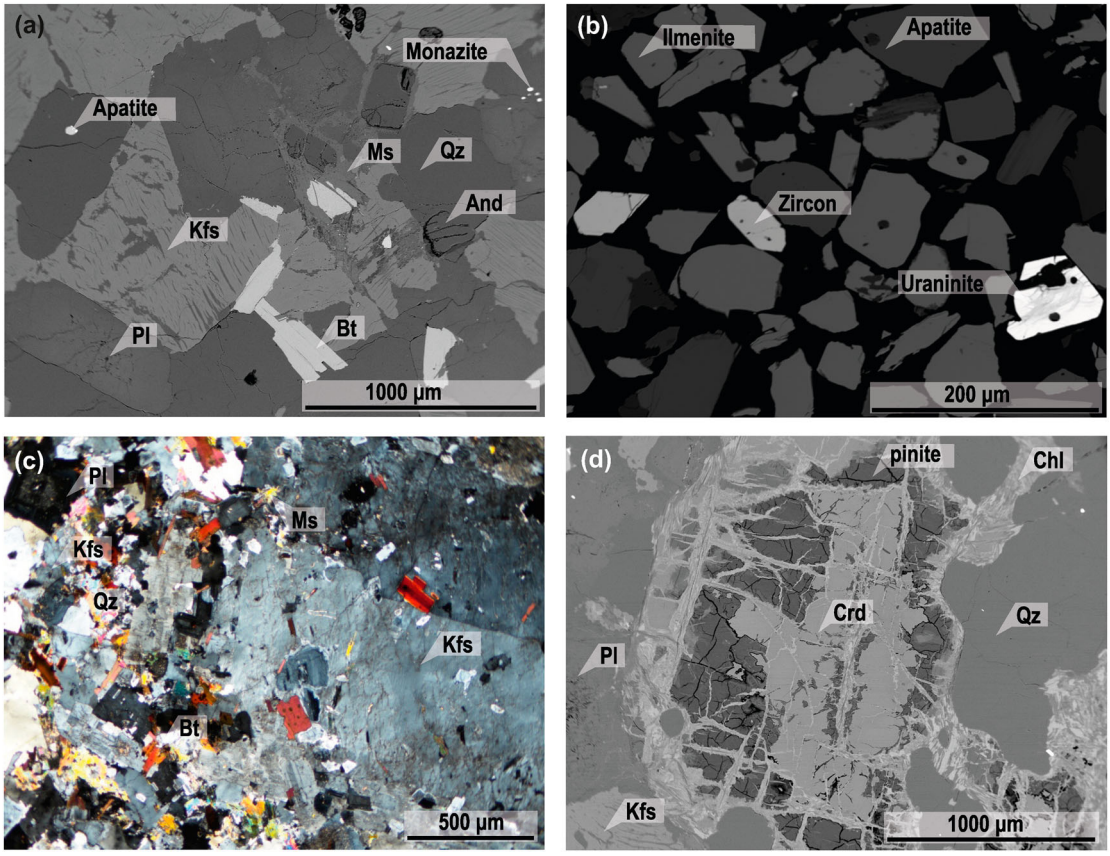

Figure 2. (a) Muscovite-biotite granite (Deštná type) with subhedral andalusite crystals (BSE image). (b) Polished heavy mineral fraction of the Deštná type granite (BSE image). (c) Porphyritic muscovite-biotite granite (Dívčí Kopy type); XPL photomicrograph. (d) Altered cordierite crystal in the Radouň type granite (BSE image). Abbreviations: Kfs: K-feldspars; Pl: plagioclase; Qz: quartz; Bt: biotite; Ms: muscovite; Crd: cordierite; Chl: chlorite.

to syenogranite (Figure 3(a)). The peraluminosity of all the represented granites is shown on the A-B diagram (Debon & Le Fort, 1983; modified by Villaseca et al., 1998). The Dívčí Kopy type is a highly peraluminous granite and the Deštná type is moderately peraluminous (Figure 3(b)). The granites of the Klenov Pluton show variable Rb/Sr ratios (in the range of 0.5–6.4) and Rb/Ba ratios (in the range of 0.1–4.6). The studied granites are also represented by a relatively variable Zr content (>7–162 ppm) and low Nb (up to 18 ppm). The chondrite-normalized REE plots (Boynton 1984) of the studied granites (Figure 3(c)) show that the Dívčí Kopy type has high LREE/HREE (La_N/Yb_N = 10.7–16.3), negative Eu anomalies (Eu/Eu* = 0.2–0.7) and total REE contents from 171 to 173 ppm. The Deštná I subtype is characterized by relatively low total REE (in the range of 33–54 ppm), low LREE/HREE (La_N/Yb_N = 3.6–7.2) and slight negative to positive Eu anomalies (Eu/Eu* ranges from 0.8 to 1.2). The Deštná II subtype is enriched in LREE relative to HREE (La_N/Yb_N = 30.3–43.8) and has high total REE contents (163–188 ppm). The Th/U ratio shows a difference among granite types of the Klenov Pluton (Figure 3(d)). In this context, the Dívčí Kopy type shows a Th/U ratio in the range of 2.0 to 2.5. The Th/U ratio in the Deštná I type subtype is relatively low (in the range of 0.1–1.8), whereas the Deštná II subtype shows higher Th/U ratio in the range of 2.9–3.9.

Airborne radiometric anomalies and ground gamma-ray spectrometric results indicate a variable radioactive element content in the granites of the Klenov Pluton. Potassium values range from 3% to 6%, eTh values from 2 to 34 ppm and eU values from 2 to 15 ppm. These results were confirmed by whole-rock chemical analyses (Figure 3(d)). The highest values of Th are recorded in fresh medium-grained, equigranular muscovite-biotite granite (Deštná II subtype) from the NW part of the Klenov Pluton (SE from Deštná village). The fresh granite of the Deštná I subtype contains significantly lower concentrations of Th in comparison to the Deštná II subtype and the Dívčí

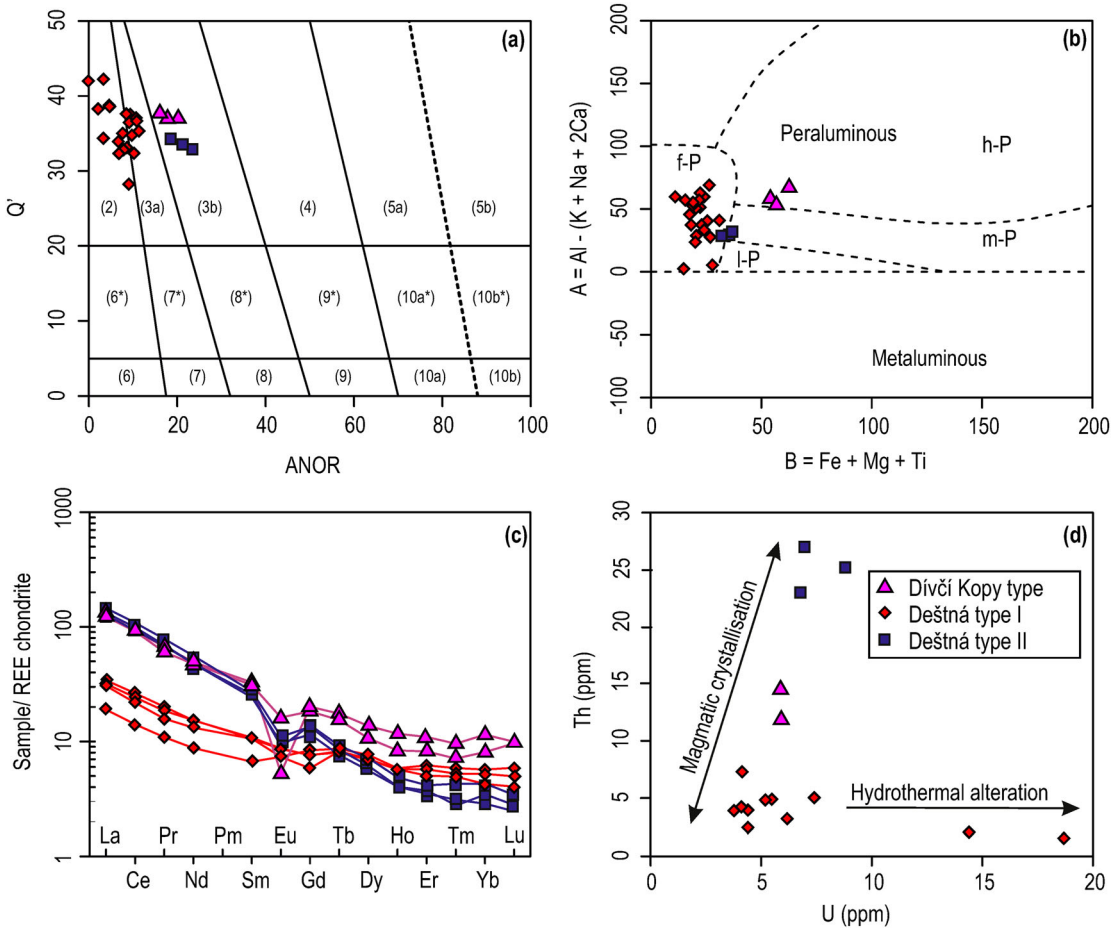

Figure 3. Selected geochemical diagrams of the granites from the Klenov Pluton. (a) ANOR vs. Q′ normative composition diagram (after Streckeisen and Le Maitre, 1979): ANOR = An × 100/(Or + An), Q′ = Q × 100/(Q + Or + Ab + An); 2 Alkali-feldspar granite, 3a Syenogranite, 3b Monzogranite, 4 Granodiorite, 5a Tonalite, 5b Calcic Tonalite, 6* Alkali-feldspar Quartz-Syenite, 7* Quartz Syenite, 8* Quartz Monzonite, 9* Quartz Monzodiorite, 10a* Quartz diorite, 10b* Quartz Gabbro, 6 Alkali-feldspar Syenite, 7 Syenite, 8 Monzonite, 9 Monzogabbro, 10a Diorite, 10b Gabbro. (b) B vs. A diagram after Villaseca et al. (1998) for distinguishing different granitic series. HP = highly peraluminous, MP = moderately peraluminous, LP = low peraluminous, FP = felsic peraluminous. (c) Chondrite (Boynton 1984) normalized REE patterns. (d) U vs. Th diagram.

Kopy type (Figure 3(d)). The U/Th ratio for the Deštná II subtype varies from 2.9 to 3.9 and is higher than the range recorded for other types of granites (0.1–2.5).

5. U-Pb monazite dating

Five monazite grains from the equigranular to weakly porphyritic Deštná Granite were broken into two fragments and dated separately by isotope dilution thermal ionization mass spectrometry (ESM-1, ESM-2; Figure 4(a)). The six oldest $^{207}Pb/^{235}U$ dates (Figure 4(b)) are similar, with a weighted mean of 328.35 ± 0.22 Ma (MSWD = 1.7) calculated using Isoplot 3.0 (Ludwig, 2003). The three youngest $^{207}Pb/^{235}U$ dates (Figure 4(b)) are the same, with a weighted mean of 327.14 ± 0.21 Ma (MSWD = 0.9). One other analysis yielded a $^{207}Pb/^{235}U$ date of 327.80 ± 0.37 Ma (white rectangle in Figure 4(b)).

6. Geophysical survey

The geophysical survey was used to identify the lithological boundaries, faults, and domains of deep weathering (Figure 5; Fig. 2a,b on Main Map). The overall geological pattern and major lithological boundaries, to a depth of several hundreds of metres, was inferred based on the gravity data. The granites of the Klenov Pluton reveal the lowest density values (2.6 g/cm^3) among all the rocks in the studied area (Blížkovský & Novotný, 1981) and form a distinct negative gravity anomaly reaching −40 mGal (Fig. 3 on Main Map). The densities of the surrounding rocks (biotite migmatites (2.66 g/cm^3) and biotite orthogneiss (2.61 g/cm^3), as reported by Blížkovský and Novotný (1981), are higher. Therefore, the overall shape of the Klenov Pluton can be readily estimated from the gravity data. The Linsser indications, calculated for the density contrast 0.06 g/cm^3 (the density difference between the granites of the Klenov Pluton and surrounding migmatites), marked distinct density boundaries (Fig. 3 on Main Map). The interpreted geological profile across the Klenov Pluton (Fig. 2c on Main Map) crosses two of these density interfaces, at 3.8 km along the profile and just behind the end of the profile at 5.1 km. The first density interface indicates a step-change in the bottom interface of the pluton, probably by movement along the fault plane. The second of these two interfaces is connected with the Lodhéřov Fault Zone where, according to the gravity model, the thickness of the pluton significantly decreases again (Fig. 2c on Main Map). The resistivity of granites is generally high (higher than approximately 1000 Ωm) whereas the resistivity of metamorphic rocks, such as migmatite and paragneiss, is lower than 300 Ωm (see profiles CIH02a and CIH04a in Figure 5). In contrast, fault zones in granites could have resistivities as low as 100 Ωm due to higher water content and more intensive weathering (e.g. Fröhlich, 1964; Hartvich & Valenta, 2013; Valenta et al., 2008). The fault zones are readily visible, especially in the ERT results (see profiles CIH02a and CIH04a in Figure 5).

The accompanying seismic survey enables a more precise interpretation of non-unique resistivity data (e.g. the same value of low resistivities could indicate either the fault zone or compact metamorphic rocks). While decreased values of P-wave velocities (below approximately 2000m/s as in this case) combined with low resistivity values indicate the presence of a fault zone, the high P-wave velocities (over approximately 3500 m/s), irrespective of the resistivity values, represent the compact rocks (see profiles CIH02b and CIH04c on Figure 5). In addition, the

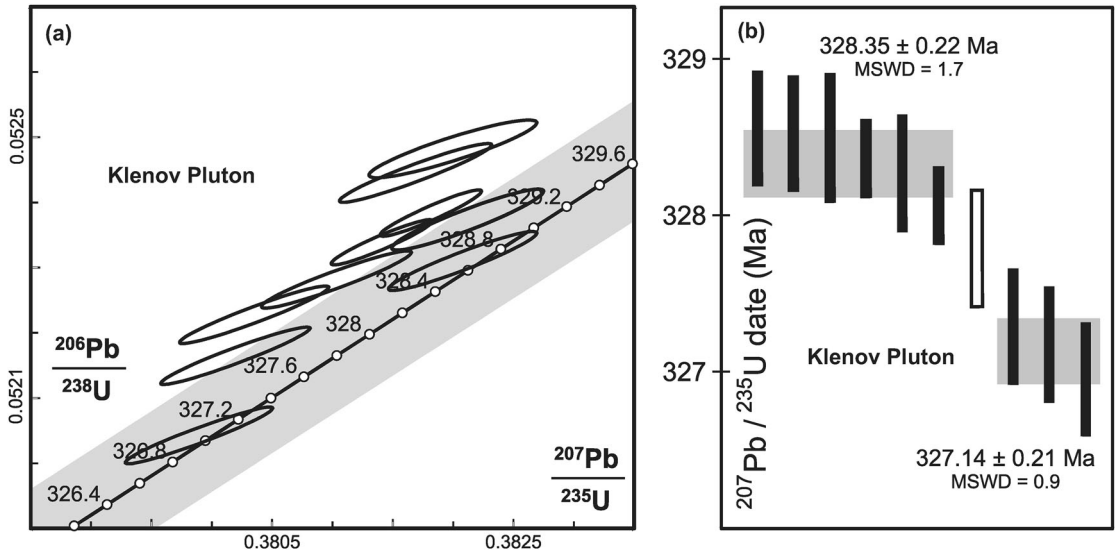

Figure 4. (g) U-Pb concordia diagram showing ages of monazite TIMS dating results; (b) Diagram of interpreted U-Pb ages in two populations of a monazite fraction.

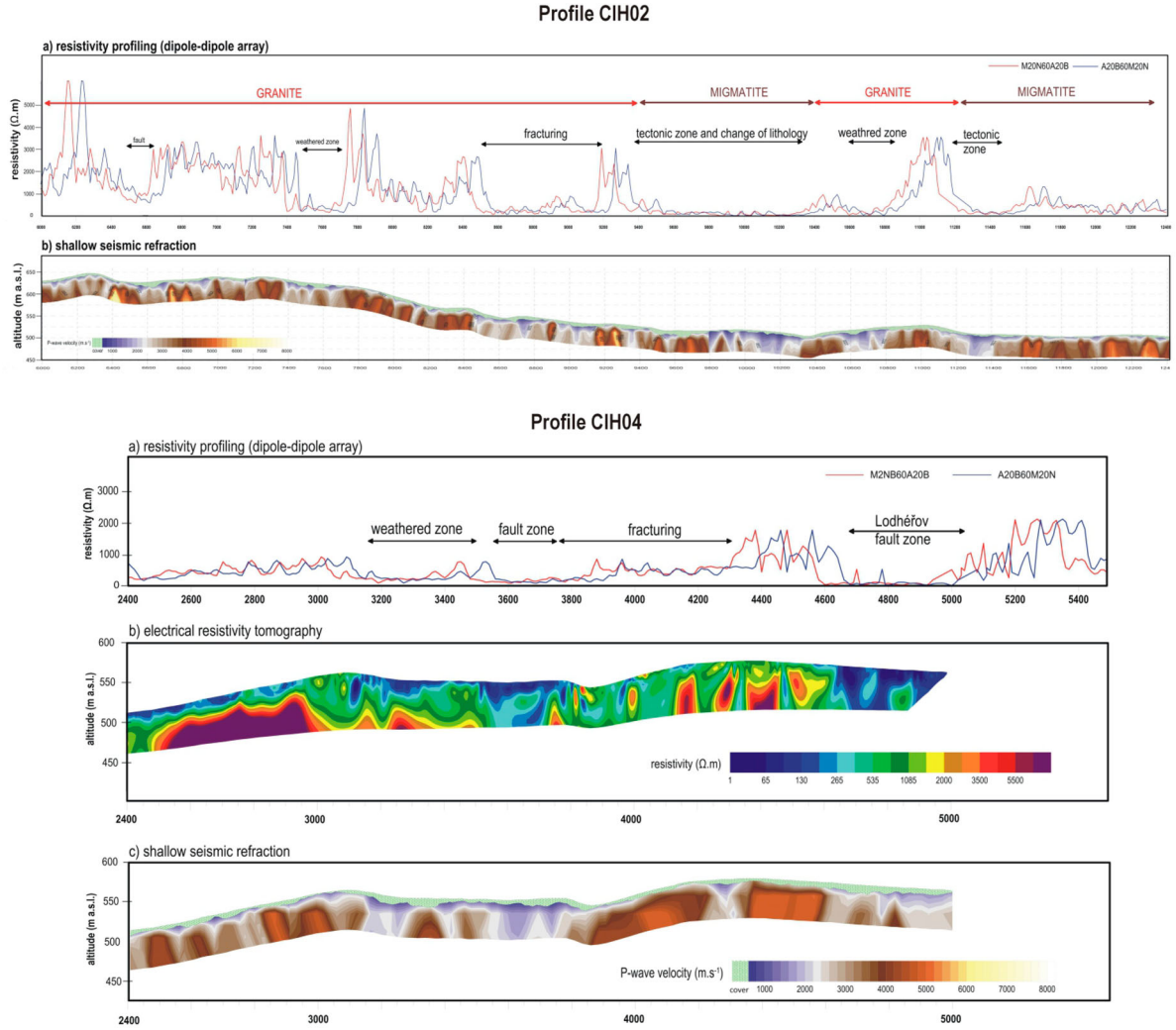

Figure 5. Geophysical anomalies and geological interpretations on the profile CIH02 (6600–12400 m) and profile CIH04 (2400–5600 m).

gamma-ray survey (gamma-ray spectrometry) contributes to a precise determination of the lithological pattern. Whereas the concentration of potassium and uranium remains mostly uniform across the surveyed area (3-4% K and 4–6 ppm U) the thorium level changes. The highest thorium concentrations in the soil environment (Th~20 ppm) were measured in the northern part of the Klenov Pluton (nearby the village of Deštná). The rest of the pluton reveals much lower Th concentrations at ca. 10 ppm (ESM-3, ESM-4). Similar results were also acquired by field measurement on the outcrops where Th concentrations in the range of 11–27 ppm were found in the northern segment of the pluton and in the range of 2–6 ppm for its other parts (ESM-5).

7. Fabric pattern

The compositional banding in the host migmatites (Figure 6(a)) dips gently to moderately to the ~NW to ~WNW (Figure 6(c)). The associated, well-developed stretching or mineral lineation formed by feldspars, biotite and sillimanite aggregates plunges gently to the ~W to ~NW or ~N(NNE). The regional foliation encloses minor rootless, closed to isoclinal folds with more variable trends of fold axes, predominantly plunging to ~NNE, ~SSW or ~W to NW. If fold axes are perpendicular to the stretching lineation, the fold asymmetry (in L-par section) reveals normal (ESE-side-up) kinematics, similar to asymmetry of mica fishs, quartz and feldspar porphyroblasts and sillimanite tails in the L-par section. The migmatites were intruded by post-collisional granites in the form of a gently to moderately ~WNW to ~NNW dipping irregular intrusive body with sheeted margins as intrusive contacts. The transitional, magmatic to HT subsolidus foliation in the Klenov Pluton (Figure 6(b)) is mostly parallel to the intrusive contacts and regional foliation in the host migmatites, dipping gently to moderately to the ~NW (Figure 6d).

The morphotectonic pattern (Figure 7; ESM-6) combined with the results of field structural analysis indicates the presence of regional faults and joints (e.g. Burbank & Anderson, 2001; Ganas et al., 2005; Jelínek, 2008). The faults were found in two orientations (Figure 6e): (a) dipping steeply to ~NE

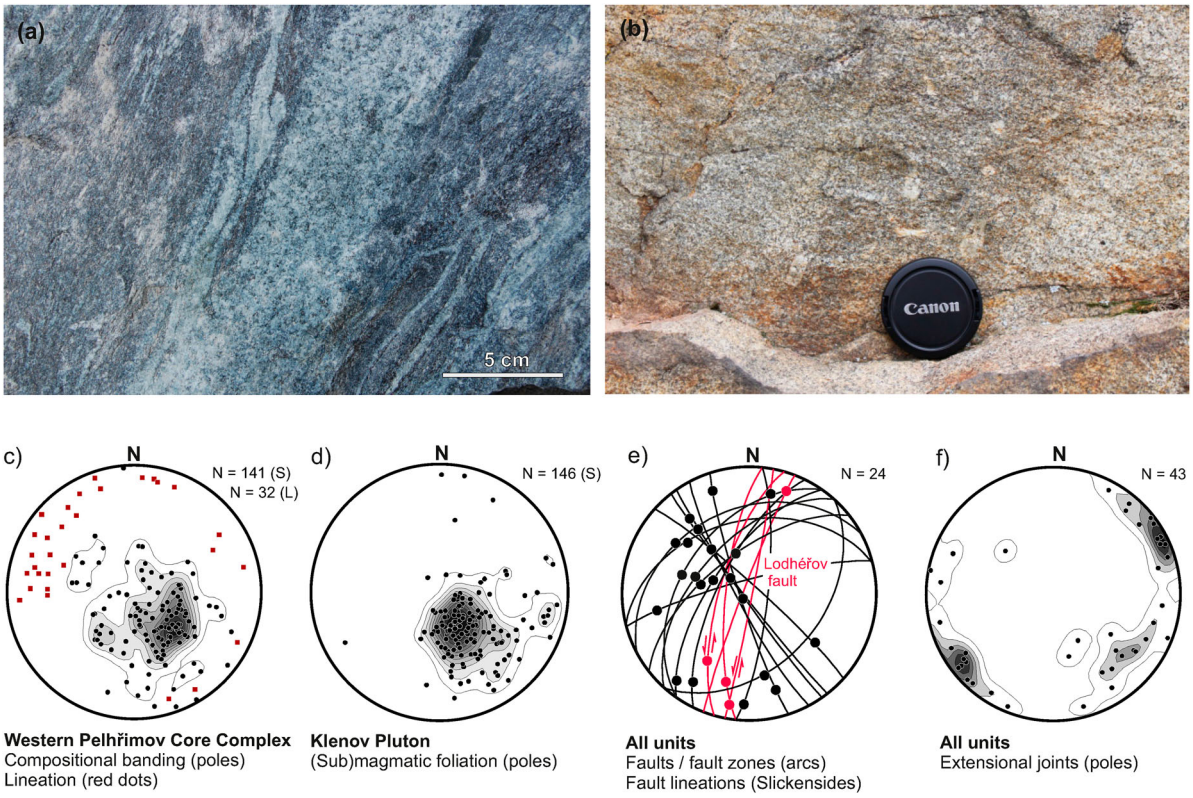

Figure 6. (a) Field photograph of compositional banding in the host migmatites of the Pelhřimov Core Complex; (b) Field photograph of transitional magmatic to submagmatic foliation in the Klenov Pluton; (c) Diagram of compositional banding (poles) in the host migmatites of the Pelhřimov Core Complex; (d) Diagram of transitional magmatic to submagmatic foliation (poles) in the Klenov Pluton; (e) Diagram of mapped faults (arcs) and associated fault lineations (slickensides); (f) Diagram of extensional joints (poles). Stereographic equal projection to lower hemisphere.

(NNE) or ~SW bearing slickensides of two generations, plunging gently to ~NW or ~SE with prevailing right-lateral kinematics and plunging steeply bearing normal kinematic indicators ~NNW(NW) to WNW steeply to moderately dipping associated with normal SE-side-up normal kinematics and slickensides plunging gently to SSW or NNE bearing the left-lateral kinematic pattern. The ~NE–SW trending faults occur mainly along the eastern edge of the Klenov Pluton, designated as the Lodhéřov Fault Zone. Two sets of extensional joints with a lack of mineral infill were identified in all lithologies (for their orientation see Figure 6(e)): (a) prevailing subvertical extensional joints trending ~WNW(NW)–ESE(SE) showing an average joint spacing in the Klenov Pluton of about 70 centimetres and (b) subordinate extensional joints trending NNE–SSW revealing an average joint spacing of about 110 centimetres.

8. Geological map of the Klenov Pluton

The geological map of the Klenov Pluton (Main Map) and host high-grade migmatites of the eastern Pelhřimov Core Complex (Moldanubian Zone) was compiled based on the results of field geological mapping on a scale of 1:10,000, an analysis of the petrological and geochemical composition of the rocks, a morphostructural and field structural analysis and the results of a geophysical survey. The host rocks are represented by biotite migmatite and migmatized paragneiss with numerous elongate bodies of orthogneiss and felsic granulite, with minor intercalations of quartzite, amphibolite and calc-silicate rocks. The regional metamorphic foliation in the host metamorphic rocks is mostly parallel to the partial lithological boundaries, dipping gently to moderately to the ~NW to ~WNW (see Fig. 2d on Main Map, ESM-7). The Klenov Pluton consists of three types of two-mica ('Eisgarn-type') granite referred as the Deštná, Radouň and Dívčí Kopy types. The contacts of the Klenov Pluton have a predominantly intrusive character, commonly forming a 'sheet-line' pattern, to regional foliation. The north-western tip of the pluton dips gently to moderately to the ~NW(NNW), whereas the eastern margin is inclined steeply to ~WNW(NW). Small, irregular xenoliths (up to metres in size) of host metamorphic rocks were found in the western part of the pluton. Numerous steeply ~NE(NNE)–SW(SSW) or ~NW–SE dipping pegmatite, leucogranite or hydrothermal quartz veins or dikes were emplaced discordantly with respect to the regional metamorphic fabrics and contacts of individual lithologies. Minor fluvial and colluvial sediments of Neogene to Quaternary age occur mainly

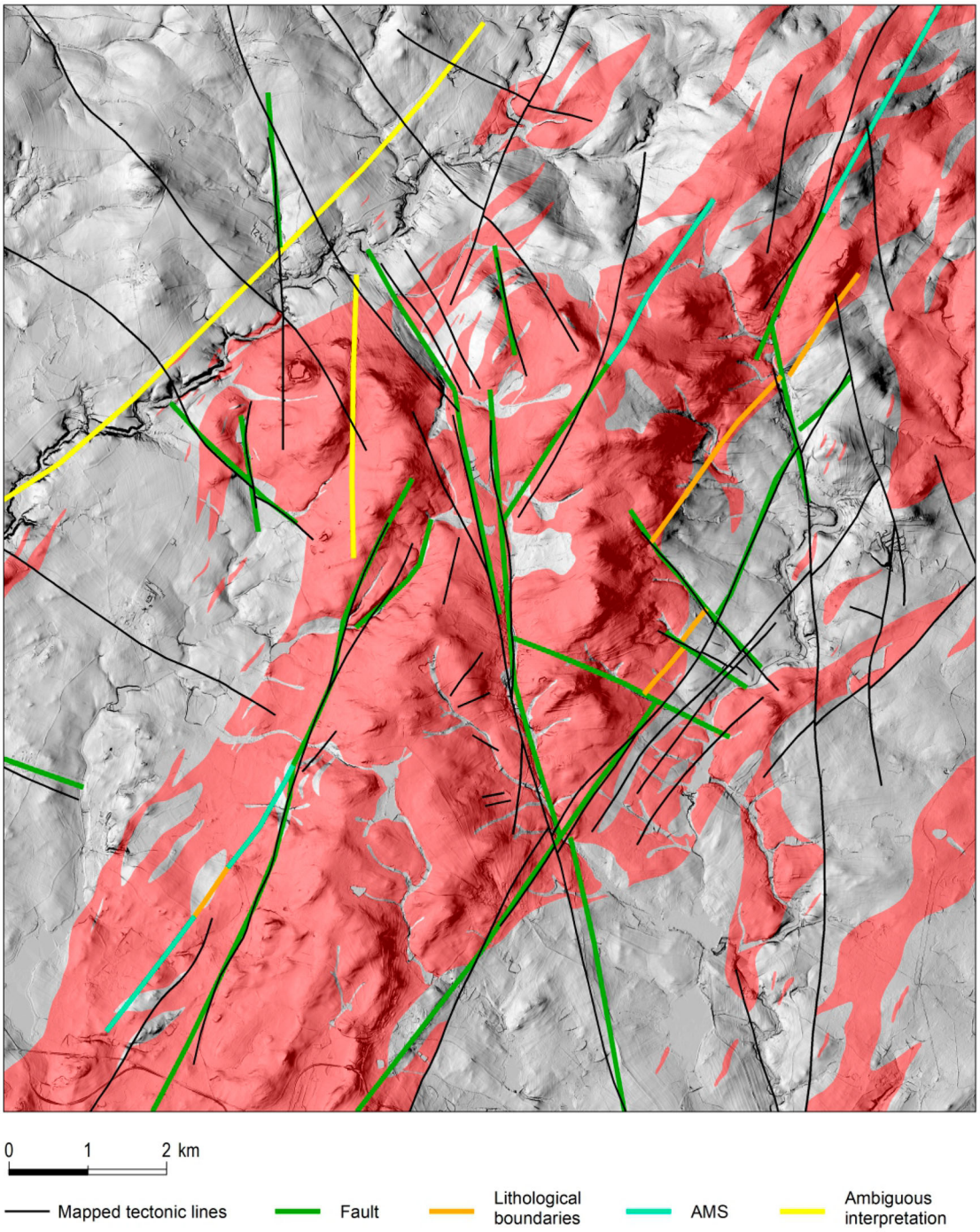

Figure 7. Schematic map of main lineaments and faults. The position of the Klenov Pluton is labelled by a red polygon.

in the form of denudation remnants in the morphological depressions and river valleys.

9. Discussion

The granites of the Klenov Pluton are peraluminous with high K_2O, Th U concentrations and K_2O/Na_2O, Rb/Sr, and Rb/Ba values, and low Zr and Nb contents. Such geochemical signatures are typical for granites generated by partial melting of metasedimentary sources (predominantly metapsamites) at very high temperatures, as previously reported by René et al. (2008); Žák et al. (2014); René (2020); Finger et al. (2022). The differences in chemical composition among individual granite (sub)types of the Klenov Pluton are seen in their variable LREE/HREE ratios, the presence of negative or positive Eu anomalies (Eu/Eu* 0.2–1.2), and their Th/U ratios (0.1–3.9). These differences (e.g. SiO_2, K_2O contents) among the individual granite types mostly reflect the different degree of differentiation of the original peraluminous melt (e.g. Tartese & Boulvais, 2010) and/or late magmatic to postmagmatic modifications (Dolníček & Krobot, 2013; René, 2005). The variable REE contents in individual granite varieties can be explained by differences in monazite, apatite, and zircon

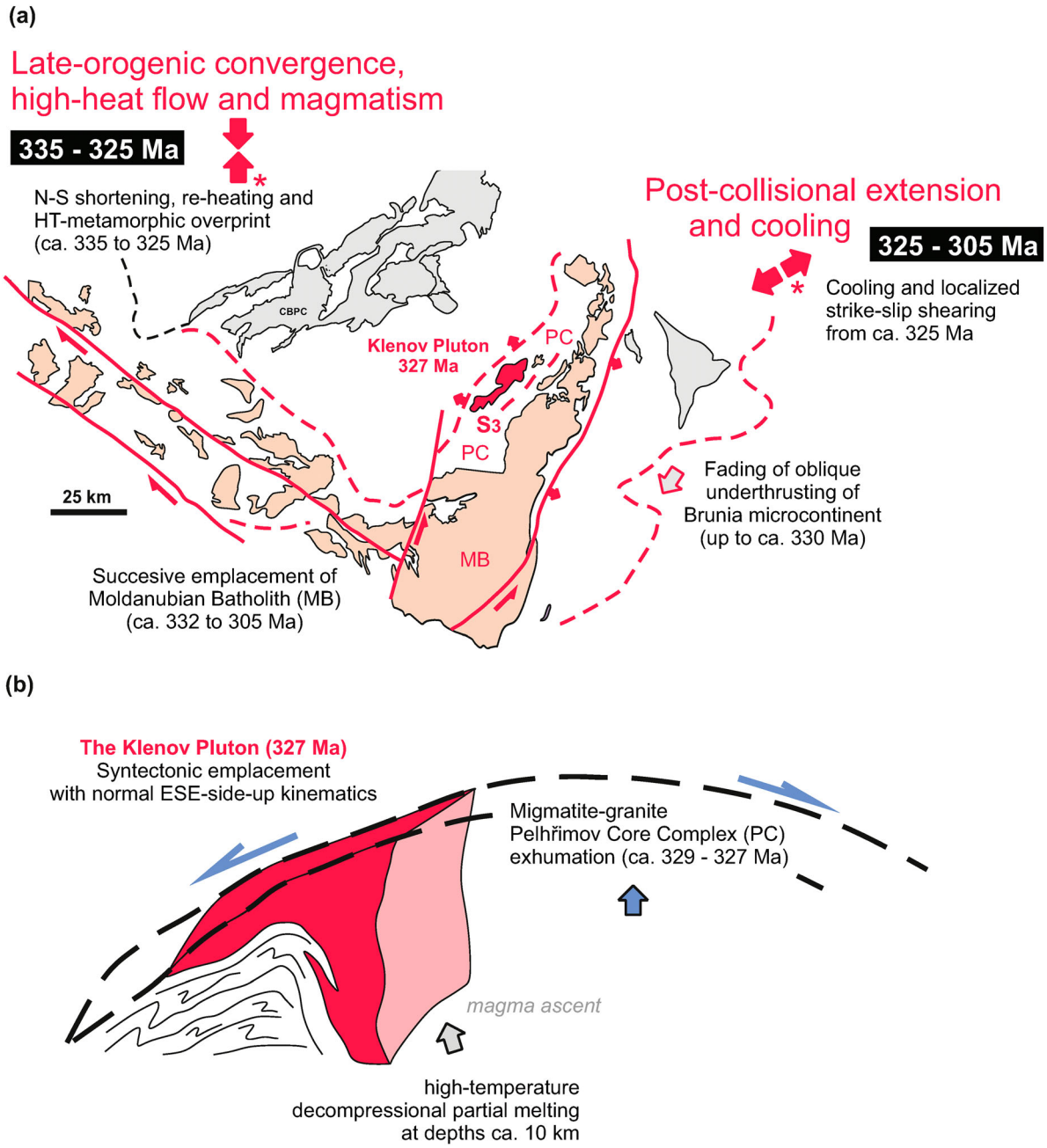

Figure 8. (a) Emplacement of the 327 Ma Klenov Pluton within the context of the geodynamic evolution of Variscan late-orogenic convergence and subsequent post-collisional extension (from ca. 335 to 325 Ma); (b) Schematic block diagram of the Klenov Pluton and host migmatite-granite Pelhřimov Core Complex.

abundances from different domains of the Klenov Pluton (Bea, 1996). The U and Th anomalies of two-mica granite (subtype Deštná II) in the ~NW part of the Klenov Pluton can be explained by the variable amounts of accessory minerals such as monazite and uraninite. The highest U contents and the lowest Th/U ratio were also detected by airborne gamma-ray spectrometry, is associated with the ~N–S to NNW–SSE oriented shear or fault zone in the vicinity of Okrouhlá Radouň village, indicates the presence of hydrothermal alteration (uraninite-coffinite mineralization) in the Okrouhlá Radouň Ore Deposit (Dolníček & Krobot, 2013; Fiala & Čadek, 1981; René, 2005). The measured ages of 327.14 ± 0.21 Ma and 327.80 ± 0.37 Ma (U-Pb TIMS dating on monazites) reflect the fast magma emplacement and crystallization of the Klenov Pluton. The crystallization age of the Klenov Pluton is thus only about 1 Ma older than the neighbouring Mrákotín Composite Pluton emplaced into the central part of the Pelhřimov Core Complex (Žák et al. 2011).

The distinct negative gravity anomaly reaching −40 mGal (Fig. 2 on Main Map) and its distribution allowed the Linsser indications to be calculated (e.g. Šefara, 1973; Verner et al., 2014), thus enabling the identification of the gravity interface orientation below the surface to a depth of approximately 2 km. In summary: (a) the western contact of the pluton

has an intrusive 'sheet-like' pattern, mostly parallel to the regional foliation dipping at moderate angles to the ~WNW(NW) beneath the host migmatites of the westernmost flank of the Pelhřimov Core Complex (Verner et al., 2014; Žák et al., 2019), and (b) The eastern boundary of the pluton is more variable, where the original steeply ~WNW dipping intrusive contact has been partly modified by the steeply to moderately ~NNE(NE)–SSW(SW) trending Lodhéřov Fault Zone with polyphase normal and left-lateral shearing. The Lodhéřov Fault Zone is a prominent tectonic structure detected by the geophysical survey as well as by conventional geological mapping. In this context, the resistivity and seismic velocity values reveal a pronounced minima there, showing a wider (at least 300 meters) tectonically affected zone (see profile CIH04 in Figure 5). The main Lodhéřov Fault Zone is probably subvertical to ca. 80° dipping to the WNW. In addition, the Linsser indications (Fig. 5 on Main Map) reveal a significant vertical movement along the Lodhéřov Fault Zone. The gravity model (Fig. 2 on Main Map) suggests that the easternmost part of the pluton (east of the Lodhéřov Fault Zone) is shallower than its western part. The overall thickness of granite decreases to approximately 1 km east of this zone (probably due to later fault activity) forming a common 'sheet-like' pattern (Main Map). The density contrast close to the eastern margin of the pluton, emphasized by Linsser indications, mark another substantial vertical density interface, where the thickness of the pluton further decreases. This interface is the result of the fault zone, which is further supported by the decrease of resistivities and seismic velocities on the Profile CIH02 (Figure 5, x-coordinates from 8600 to 9100 m). Based on the approximation of the orientation of the intrusive contacts, it is possible to assume that the greatest vertical extent of the granites achieved along the western margin of the pluton would be at least 5 kilometres. This assumption is further supported by the Bouger anomaly map (Fig. 2 on Main Map) where the corresponding density minima along the western contact of the pluton were identified. The 3D visualization reveals the overall geological pattern of the Klenov Pluton and its surrounding high-grade host rocks. Unlike common geological models displaying the 3D shape of geological bodies (e.g. Høyer et al., 2015; Thornton et al., 2018), the presented 3D visualization was constructed manually, taking into account the detailed information at each point of the model.

These new findings, regarding the Klenov Pluton as an integral part of the Pelhřimov Core Complex (asymmetrical migmatite-granite domal structure dated at ca. 329 to 327 Ma; e.g. Verner et al., 2014; Žák et al. 2011, 2019), allows for the interpretation of pluton emplacement in the context of the Variscan, late-orogenic paleostress conditions (Figure 8(a)). The regional ~N–S shortening in a collisional regime associated with additional heating, the intense (re)melting of metasedimentary crustal sources, and an HT-metamorphic overprint took place within the time span of ca. 335 to 325 Ma (Edel et al., 2018; Megerssa et al., 2022). Synchronously oblique, ~NNE–SSW oriented underthrusting of the Brunia microcontinent beneath the eastern Moldanubian Zone was terminated at ca. 330 Ma (e.g. Racek et al., 2017; Verner et al., 2014). These processes were followed by regional ~ENE–WSW oriented post-collisional extension and cooling at ca. 325 to 305 Ma (Edel et al., 2018). In this context, the 327 Ma Klenov Pluton is interpreted as a syntectonic, 'sheet-like' intrusion emplaced during the later stages of Pelhřimov Core Complex exhumation (Figure 8(b)), and affected by ~N–S oriented compression (transpression) that followed the termination of obligue underthrusting of the Brunia microcontinent (Edel et al., 2018; Megerssa et al., 2022). The overall asymmetric shape of the pluton, as well as its fabric pattern roughly similar to the surrounding migmatites, was later modified by polyphase normal SE-side-up normal and left-lateral faulting along its eastern margin (Lodhéřov Fault Zone). This study contributes to the understanding and significance of magmatism in the late-orogenic stages of compressional orogenic belts, which is the subject of current discussions (e.g. Bolle et al., 2023; Gardien et al., 2022 and references therein).

10. Conclusions

The new geological map of the Klenov Pluton, on a scale of 1:30,000, and its 3D visualization, compiled using a wide range of field, analytical, and geophysical data, provide broad implications for subsequent applied research as well as new knowledge regarding granite emplacement within a late-orogenic geodynamic context. The Klenov Pluton has a peraluminous composition resulting from partial melting of metasedimentary sources at depths of ca. 10 km. The crystallization ages of 327.14 ± 0.21 Ma and 327.80 ± 0.37 Ma (U-Pb TIMS dating on monazites) reflect the short time span of granite magma emplacement and cooling. The 327 Ma Klenov Pluton was emplaced syntectonically as a 'sheet-like' granite intrusion, during the later stages of the Pelhřimov Core Complex's exhumation path (at ca. 329 to 327 Ma) in the interplay with regional ~N–S oriented compression. Gravity modelling suggests that the Klenov Pluton has an asymmetric shape where its western flank (ca. 5 km of depth) is parallel to the ~NW moderately dipping Pelhřimov Core Complex. The eastern margin of the Pluton is much shallower (ca. 1 km of depth) and has been later modified by ~SE-side-up normal faulting (Lodhéřov Fault Zone).

Software

The Esri ArcGIS software was used for the Main Map construction and spatial data processing. The spatial data used for the map are stored as Esri file geodatabase (*.gdb). Geophysical survey outputs were visualised in Surfer (Golden Software). The morphostructural analyses were performed using ArcGIS and Surfer. CorelDRAW, ArcGIS and Surfer were used for drafting the figures. The data for the 3D model were prepared in ArcGIS and modelled in MOVE (Petroleum Experts).

Acknowledgements

The study was funded by Research Project No. 310940 to J. Pertoldová (Strategic Research Plan of Czech Geological Survey 2018–2022), the Czech Science Foundation (Grant No. 15-34621L to K. Verner) and SURAO project 'Update of 3D structural geological models of potential sites of a deep repository for radioactive waste'. We gratefully acknowledge Mr. Tomas Hroch for the field assistance and the reviewers Dr. Luana Florisbal, Dr. Mike Shand and Dr. Valdecir Janasi, for their careful review of the manuscript and constructive comments.

Disclosure statement

No potential conflict of interest was reported by the authors.

Data availability statement

The authors of this publication confirm that all the geological field and analytical data, as well as the results of the geophysical survey, are available within the article and its supplementary material (ESM) and are unique and clearly support all the findings.

References

Bea, F. (1996). Residence of REE, Y, Th and U in granites and crustal protoliths; implications for the chemistry of crustal melts. *Journal of Petrology*, *37*(3), 521–552. doi:10.1093/petrology/37.3.521

Blížkovský, M., & Novotný, A. (1981). Construction of stripped gravity map of the Bohemian Massif. *Geophysical Syntheses in Czechoslovakia*, *26*, 103–110.

Bolle, O., Corsini, M., Diot, H., Laurent, O., & Melis, R. (2023). Late-orogenic evolution of the Southern European Variscan Belt constrained by fabric analysis and dating of the Camarat Granitic Complex and coeval felsic dykes (Maures–Tanneron Massif, SE France). *Tectonics*, *42*(4), 1–35.

Bouchez, J. L., Hutton, D., & Stephens, W. E. (eds.). (2013). *Granite: From segregation of melt to emplacement fabrics* (Vol. 8). Springer Science & Business Media.

Boynton, W V. (1984). Cosmochemistry of the rare earth elements: meteorite studies. In *Developments in geochemistry* (Vol. 2, pp. 63–114). Elsevier.

Brandmayer, M., Dallmeyer, R. D., Handler, R., & Wallbrecher, E. (1995). Conjugate shear zones in the Southern Bohemian Massif (Austria): implications for Variscan and Alpine tectonothermal activity. *Tectonophysics*, *248*(1-2), 97–116. doi:10.1016/0040-1951(95)00003-6

Burbank, D. W., & Anderson, R. S. (2001). Geomorphic markers. In D. W. Burbank, & R. S. Anderson (Eds.), *Tectonic geomorphology* (pp. 13–32). Blackwell Publishing.

Castro, A., Patiño Douce, A. E., Corretgé, L. G., De La Rosa, J. D., El-Biad, M., & El-Hmidi, H. (1999). Origin of peraluminous granites and granodiorites, Iberian Massif, Spain: An experimental test of granite petrogenesis. *Contributions to Mineralogy and Petrology*, *135*(2–3), 255–276. doi:10.1007/s004100050511

Chandrasekharam, D., & Ranjith Pathegama, G. (2020). CO_2 emissions from renewables: Solar pv, hydrothermal and EGS sources. *Geomechanics and Geophysics for Geo-Energy and Geo-Resources*, *6*(1), 1–17. doi:10.1007/s40948-019-00135-y

Chen, M., Tompson, A. F., Mellors, R. J., & Abdalla, O. (2015). An efficient optimization of well placement and control for a geothermal prospect under geological uncertainty. *Applied Energy*, *137*, 352–363. doi:10.1016/j.apenergy.2014.10.036

Debon, F., & Le Fort, P. (1983). A chemical–mineralogical classification of common plutonic rocks and associations. *Transactions of the Royal Society of Edinburgh: Earth Sciences*, *73*(3), 135–149. doi:10.1017/S0263593300010117

Dolníček, Z., & Krobot, J. (2013). Garnet-calcite vein mineralization in contact-metamorphosed sandstones from Bučník near Komňa (Bílé Karpaty Unit). *Geologické výzkumy na Moravě a ve Slezsku*, *2*, 1–2.

Edel, J. B., Schulmann, K., & Holub, F. V. (2003). Anticlockwise and clockwise rotations of the Eastern Variscides accommodated by dextral lithospheric wrenching: palaeomagnetic and structural evidence. *Journal of the Geological Society*, *160*(2), 209–218. doi:10.1144/0016-764902-035

Edel, J. B., Schulmann, K., Lexa, O., & Lardeaux, J. M. (2018). Late Palaeozoic palaeomagnetic and tectonic constraints for amalgamation of Pangea supercontinent in the European Variscan belt. *Earth-science Reviews*, *177*, 589–612. doi:10.1016/j.earscirev.2017.12.007

Eshaghi, E., Reading, A. M., Roach, M., Duffett, M., Bombardieri, D., Cracknell, M. J., & Everard, J. L. (2020). Efficient regional scale 3D potential field geophysical modelling to redefine the geometry of granite bodies beneath prospective, geologically complex, northwest Tasmania. *Ore Geology Reviews*, *127*, 103799. doi:10.1016/j.oregeorev.2020.103799

Feng, G., Wang, X., Wang, M., & Kang, Y. (2020). Experimental investigation of thermal cycling effect on fracture characteristics of granite in a geothermal-energy reservoir. *Engineering Fracture Mechanics*, *235*, 107180. doi:10.1016/j.engfracmech.2020.107180

Fiala, J., Fuchs, G., & Wendt, J. I. (1995). *Pre-Permian geology of central and Eastern Europe* (Vol. 7, pp. 417–428). Springer Berlin Heidelberg.

Fiala, V., & Čadek, J. (1981). Hydrothermal alterations at the deposit Okrouhlá Radouň. Sborn Geol Věd Lož. *Geol Mineral*, *22*, 159–199.

Finger, F., Gerdes, A., Janoušek, V., René, M., & Riegler, G. (2007). Resolving the Variscan evolution of the Moldanubian sector of the Bohemian Massif: The significance of the Bavarian and the Moravo-Moldanubian tectonometamorphic phases. *Journal of Geosciences*, *52*(1-2), 9–28.

Finger, F., Schiller, D., Lindner, M., Hauzenberger, C., Verner, K., & Žák, J. (2022). Ultrahigh-temperature granites and a curious thermal eye in the post-collisional South Bohemian batholith of the Variscan orogenic belt (Europe). *Geology*, *50*(5), 542–546. doi:10.1130/G49645.1

Franke, W. (1989). Tectonostratigraphic units in the Variscan belt of central Europe. *Geol Soc Am Spec Pap*, *230*, 67–90.

Franke, W. (2000). The middle-European segment of the Variscides: Tectonostratigraphic units, terrane boundaries and plate tectonic evolution. In W. Franke, U. Haak, O. Oncken, & D. Tanner (Eds.), *Orogenic processes: Quantification and modelling in the Variscan belt* (Vol. 179, pp. 35–61). Geol. Soc. London Spec. Publ.

Fröhlich, R. K. (1964). Geoelectrical measurements on a fault in the tertiary basin of Mainz (Germany), using the four point method. *Geoexploration*, *2*(3), 175–184. doi:10.1016/0016-7142(64)90009-2

Ganas, A., Pavlides, S., & Karastathis, V. (2005). DEM-based morphometry of range-front escarpments in Attica, central Greece, and its relation to fault slip rates. *Geomorphology*, *65*(3-4), 301–319. doi:10.1016/j.geomorph.2004.09.006

Gardien, V., Martelat, J. E., Leloup, P. H., Mahéo, G., Bevillard, B., Allemand, P., Monié, P., Paquette, J. L., Grosjean, A. S., Faure, M., & Chelle-Michou, C. (2022). Fast exhumation rate during late orogenic extension: The new timing of the Pilat detachment fault (French Massif Central, Variscan belt). *Gondwana Research*, *103*, 260–275. doi:10.1016/j.gr.2021.10.007

Hartvich, F., & Valenta, J. (2013). Tracing an intra-montane fault: An interdisciplinary approach. *Surveys in Geophysics*, *34*(3), 317–347. doi:10.1007/s10712-012-9216-9

Høyer, A. S., Jørgensen, F., Sandersen, P. B. E., Viezzoli, A., & Møller, I. (2015). 3D geological modelling of a complex buried-valley network delineated from borehole and AEM data. *Journal of Applied Geophysics*, *122*, 94–102. doi:10.1016/j.jappgeo.2015.09.004

Jelínek, J. (2008). Morphotectonic analysis of digital relief model – A suitable means of searching for zones of rock mass brittle failure. *GeoScience Engineering*, *3*, 1–13.

Kalvoda, J., Bábek, O., Fatka, O., Leichmann, J., Melichar, R., Nehyba, S., & Spacek, P. (2008). Brunovistulian terrane (Bohemian Massif, Central Europe) from late Proterozoic to late Paleozoic: A review. *International Journal of Earth Sciences*, *97*(3), 497–518. doi:10.1007/s00531-007-0183-1

Klomínský, J., Jarchovský, T., & Rajpoot, G. S. (2010). *Atlas of plutonic rocks and orthogneisses in the Bohemian Massif*. Czech Geological Survey.

Košler, J., Konopásek, J., Sláma, J., & Vrána, S. (2014). U-Pb zircon provenance of Moldanubian metasediments in the Bohemian Massif. *Journal of the Geological Society*, *171*(1), 83–95. doi:10.1144/jgs2013-059

Linsser, H. (1967). Investigation of Tectonics by Gravity Detailing. *Geophysical Prospecting*, *15*(3), 480–515. doi:10.1111/j.1365-2478.1967.tb01800.x

Ludwig, K. R. (2003). User's manual for isoplot 3.00, a geochronlogical toolkit for microsoft excel. *Berkeley Geochronology Center Special Publication*, *4*, 25–32.

Matte, P., Maluski, H., Rajlich, P., & Franke, W. (1990). Terrane boundaries in the Bohemian Massif: Result of large-scale Variscan shearing. *Tectonophysics*, *177*(1-3), 151–170. doi:10.1016/0040-1951(90)90279-H

Mattila, J., & Viola, G. (2014). New constraints on 1.7 Gyr of brittle tectonic evolution in southwestern Finland derived from a structural study at the site of a potential nuclear waste repository (Olkiluoto Island). *Journal of Structural Geology*, *67*, 50–74. doi:10.1016/j.jsg.2014.07.003

Megerssa, L., Verner, K., Buriánek, D., Pour, O., Tomek, F., Schiller, D., & Martínek, K. (2022). The late-Variscan high-temperature collisional episode in the southwestern Moldanubian Zone (Bohemian Massif). *International Journal of Earth Sciences*, *112*(2), 631–658.

Racek, M., Lexa, O., Schulmann, K., Corsini, M., Štípská, P., & Maierová, P. (2017). Re-evaluation of polyphase kinematic and 40Ar/39Ar cooling history of Moldanubian hot nappe at the eastern margin of the Bohemian Massif. *International Journal of Earth Sciences*, *106*(2), 397–420. doi:10.1007/s00531-016-1410-4

René, M. (1999). Radioelement distribution and heat production of two-mica monzogranites from the Moldanubian Batholith of the Bohemian Massif (Czech Republic). *Acta Montana*, *114*, 55–66.

René, M. (2005). Geochemical constraints of hydrothermal alterations of two-mica granites of the Moldanubian Batholith at the Okrouhlá Radouň uranium deposit. *Acta Geodynamica et Geromaterialia*, *2*, 63–80.

René, M. (2020). *Geochemistry of granitic rocks of the Moldanubian Batholith (Central European Variscides)*. Geochemistry, IntechOpen.

René, M., Holtz, F., Luo, C., Beermann, O., & Stelling, J. (2008). Biotite stability in peraluminous granitic melts: Compositional dependence and application to the generation of two-mica granites in the South Bohemian batholith (Bohemian Massif, Czech Republic). *Lithos*, *102*(3-4), 538–553. doi:10.1016/j.lithos.2007.07.022

Schulmann, K., & Gayer, R. (2000). A model for a continental accretionary wedge developed by oblique collision: The NE Bohemian Massif. *Journal of the Geological Society*, *157*(2), 401–416. doi:10.1144/jgs.157.2.401

Schulmann, K., Konopásek, J., Janoušek, V., Lexa, O., Lardeaux, J. M., Edel, J. B., Štípská, P., & Ulrich, S. (2009). An Ardean type Paleozoic convergence in the Bohemian Massif. *Comptes Rendus - Geoscience*, *341*(2-3), 266–286.

Šefara, J. (1973). Interpretation of vertical density interfaces using a map of gravity anomalies by means of digital computer. *Sbor geol Věd, Už Geofyz*, *11*, 19–29.

Shao, S., Ranjith, P. G., Wasantha, P. L. P., & Chen, B. K. (2015). Experimental and numerical studies on the mechanical behaviour of Australian Strathbogie granite at high temperatures: An application to geothermal energy. *Geothermics*, *54*, 96–108. doi:10.1016/j.geothermics.2014.11.005

Soejono, I., Bukovská, Z., Levá, B., Skácelová, Z., Hejtmánková, P., Guy, A., & Urík, J. (2021). Interdisciplinary geoscientific approach to radioactive waste repository site selection: The Březový potok site, southwestern Czech Republic. *Journal of Maps*, *17*(2), 741–749. doi:10.1080/17445647.2021.2004942

Štípská, P., Schulmann, K., & Kröner, A. (2004). Vertical extrusion and middle crustal spreading of omphacite granulite: A model of syn-convergent exhumation (Bohemian Massif, Czech Republic). *Journal of Metamorphic Geology*, *22*(3), 179–198. doi:10.1111/j.1525-1314.2004.00508.x

Streckeisen, A., Maitre, Le. (1979). A chemical approximation to the modal QAPF classification of the igneous rocks. *Neues Jahrbuch fur Mineralogie*, *136*, 169–206.

Tajčmanová, L., Konopásek, J., & Schulmann, K. (2006). Thermal evolution of the orogenic lower crust during exhumation within a thickened Moldanubian root of

the Variscan belt of Central Europe. *Journal of Metamorphic Geology*, *24*(2), 119–134. doi:10.1111/j.1525-1314.2006.00629.x

Tartese, R., & Boulvais, P. (2010). Differentiation of peraluminous leucogranites "en route" to the surface. *Lithos*, *114*(3-4), 353–368. doi:10.1016/j.lithos.2009.09.011

Thornton, J. M., Mariethoz, G., & Brunner, P. (2018). A 3D geological model of a structurally complex Alpine region as a basis for interdisciplinary research. *Scientific Data*, *5*(1), 1–20. doi:10.1038/sdata.2018.238

Tóth, T. M. (2018). Fracture network characterization using 1D and 2D data of the Mórágy Granite body, southern Hungary. *Journal of Structural Geology*, *113*, 176–187. doi:10.1016/j.jsg.2018.05.029

Valenta, J., Stejskal, V., & Štěpančíková, P. (2008). Tectonic pattern of the Hronov-Poříčí trough as seen from pole-dipole geoelectrical measurements. *Acta Geodynamica et Geomaterialia*, *5*, 185–195.

Verner, K., Žák, J., Pertoldová, J., Šrámek, J., Sedlák, J., Trubač, J., & Týcová, P. (2009). Magmatic history and geophysical signature of a post-collisional intrusive center emplaced near a crustal-scale shear zone: The Plechý granite pluton (Moldanubian Batholith, Bohemian Massif). *International Journal of Earth Sciences*, *98*(3), 517–532. doi:10.1007/s00531-007-0285-9

Verner, K., Žák, J., Šrámek, J., Paclíková, J., Zavřelová, A., Machek, M., Finger, F., & Johnson, K. (2014). Formation of elongated granite–migmatite domes as isostatic accommodation structures in collisional orogens. *Journal of Geodynamics*, *73*, 100–117. doi:10.1016/j.jog.2013.10.002

Villaseca, C., Barbero, L., & Herreros, V. (1998). A re-examination of the typology of peraluminous granite types in intracontinental orogenic belts. *Transactions of the Royal Society of Edinburgh: Earth Sciences*, *89*(2), 113–119. doi:10.1017/S0263593300007045

Vondrovic, L., Augusta, J., & Vokal, A. (2021). Multicriterial site assesment of potential deep geological repository sites in Czech Republic: Integration of safety. *Technical Feasibility and Environmental Approach* (No. IAEA-CN--294).

Wang, J., Chen, L., Su, R., & Zhao, X. (2018). The Beishan underground research laboratory for geological disposal of high-level radioactive waste in China: Planning, site selection, site characterization and in situ tests. *Journal of Rock Mechanics and Geotechnical Engineering*, *10*(3), 411–435. doi:10.1016/j.jrmge.2018.03.002

Winchester, J. A., Pharaoh, T. C., & Verniers, J. (2002). Palaeozoic amalgamation of Central Europe: An introduction and synthesis of new results from recent geological and geophysical investigations. *Geological Society, London, Special Publications*, *201*(1), 1–18. doi:10.1144/GSL.SP.2002.201.01.01

Žák, J., Verner, K., Finger, F., Faryad, S. W., Chlupáčová, M., & Veselovský, F. (2011). The generation of voluminous S-type granites in the Moldanubian unit, Bohemian Massif, by rapid isothermal exhumation of the metapelitic middle crust. *Lithos*, *121*(1-4), 25–40.

Žák, J., Verner, K., Janoušek, V., Holub, F., Kachlík, V., Finger, F., & Trubač, J. (2014). A plate-kinematic model for the assembly of the Bohemian Mass if constrained by structural relationships around granitoid plutons. *Geological Society, London, Special Publications*, *405*(1), 169–196. doi:10.1144/SP405.9

Žák, J., Verner, K., Ježek, J., & Trubač, J. (2019). Complex mid-crustal flow within a growing granite–migmatite dome: An example from the Variscan belt illustrated by the anisotropy of magnetic susceptibility and fabric modelling. *Geological Journal*, *54*(6), 3681–3699. doi:10.1002/gj.3335